Modulation of porosity in a solid material enabled by bulk photoisomerization of an overcrowded alkene.

Fabio Castiglioni[1,†], Wojciech Danowski[2,†], Jacopo Perego[1], Franco King-Chi Leung[2], Piero Sozzani[1], Silvia Bracco[1], Sander J. Wezenberg[2,*], Angiolina Comotti[1,*], Ben L. Feringa[2,*]

Correspondence: S.J.Wezenberg@lic.leidenuniv.nl, Angiolina.Comotti@unimib.it, B.L.Feringa@rug.nl

1 Department of Materials Science, University of Milano Bicocca, Via R. Cozzi 55, Milano, Italy

2 Centre for Systems Chemistry, Stratingh Institute for Chemistry, University of Groningen, Nijenborgh 4, 9747 AG, Groningen, The Netherlands.

† These authors contributed equally

Abstract: Incorporation of photoswitchable molecules into solid state materials hold promise for fabrication of the responsive materials, the properties of which can be controlled on-demand. However, the possible applications of these materials are limited, due to the restrictions imposed by the solid state environment on the incorporated photoswitches, which render the photoisomerization inefficient. Here we present responsive porous switchable framework materials based on a bistable chiroptical overcrowded alkene incorporated in the backbone of the rigid aromatic framework. Due to the high intrinsic porosity, the resulting framework readily responds to a light stimulus as demonstrated by solid-state Raman and reflectance spectroscopies. Solid state ^{13}C NMR spectroscopy highlights efficient and quantitative bulk photoisomerization of the incorporated light-responsive overcrowded olefins in the solid material. Taking advantage of the quantitative photoisomerization, the porosity of the framework, and as a consequence gas adsorption, can be reversibly modulated in response to light and heat.

Inspired by biological systems, a vast number of artificial molecular machines and switches, capable of elaborate structural dynamics, have been developed.[1–4] However, in solution stimulated molecular motion is inevitably overwhelmed by isotropic thermal noise which thereby precludes any form of collective action and the extraction of macroscopic work, since the molecules behave independently from one another.[5–7] On the contrary, solid state organization can translate stimuli-controlled nanoscopic changes into useful material properties and preludes to practical outputs. Thus, a challenging endeavour of current research is to organize molecular machines and switches in the solid state to impede random, thermal motion and amplify mechanical effects along multiple length scales: this effort requires reliable strategies, allowing for restricting random motion and limiting the degrees of freedom to selected modes, without impairment of the rotary or switching functions.[8–10]

One strategy to achieve these goals is the use of solid porous materials[11–15] which can incorporate switchable moieties and provide the free volume essential for unhindered dynamics, thereby serving as a static scaffold for the flexible components. Indeed, it was demonstrated recently that molecular rotors[16–23], shuttles[24], switches[25] and motors[26] can display their designed motion while incorporated

in porous architectures. The incorporation of photoresponsive molecular switches in solid materials, on the other hand, opens new opportunities to enrich the properties of these materials in a non-invasive manner with high spatiotemporal precision.[27,28] This notion was illustrated in pioneering studies on photoresponsive porous solids functionalized with azobenzenes[29–39], dithienylethenes[40–48] or spiropyrans[49-51] showing photomodulation of gas uptake, diffusion, or guest release. However, apart from geometrical constraints, the photoisomerization in solids suffers from poor light penetration depth, and is therefore limited to the near-surface region, while the bulk of the material remains unaffected, compromising the development and future applications of these materials. As a consequence, photoswitching in bulk solid materials has only been reported for porous molecular crystals sustained by soft interactions[29] and few flexible MOFs bearing struts derived from dithienylethenes[42,45], which are prone to efficient light-induced electrocyclization, due to its small excluded-volume change, even in densely packed molecular crystals.[48] Hence, attaining bulk photoresponsivity, involving large structural motion, in robust solid materials remains a fundamental challenge.

Chiral overcrowded alkenes constitute a unique class of molecular photoswitches which exhibit a stereogenic centre in the vicinity of the olefinic bond. The steric congestion present in the system forces the molecule to adopt helical chirality, which is inverted in the photochemically generated metastable isomer (Figure 1a).[52,53] With appropriate structural modification the thermal stability of the metastable isomer can be increased by many orders of magnitude up to the point that unidirectional rotation is inhibited and the molecule can be operated as a chiral bistable switch.[54] Previously, incorporation of overcrowded alkenes in soft matter matrixes[55–60], or their anchoring to a surface[61] allowed for fabrication of materials showing unique, dynamic properties. Here we report incorporation of an overcrowded alkene bistable chiroptical switch in highly stable porous organic frameworks sustained by covalent bonds, herein referred to as porous switchable frameworks (PSFs), allowing for the switching of porosity and hence gas uptake. The overcrowded alkene was integrated into the framework backbone via its fluorenyl (stator) moiety, leaving the naphthyl moiety (rotor) as pendant (Figure 1b). In the resulting architecture, the PSF backbone serves as a rigid scaffold for the switchable unit, thereby separating rigidity of the framework from the light-controlled large amplitude motion of the naphthyl moiety of the photoswitch. The high intrinsic porosity of the PSF-type materials alleviates the constraints imposed by the solid environment on the molecular motion and allows for bulk photoisomerization in the solid state as well as photomodulation of the materials porosity.

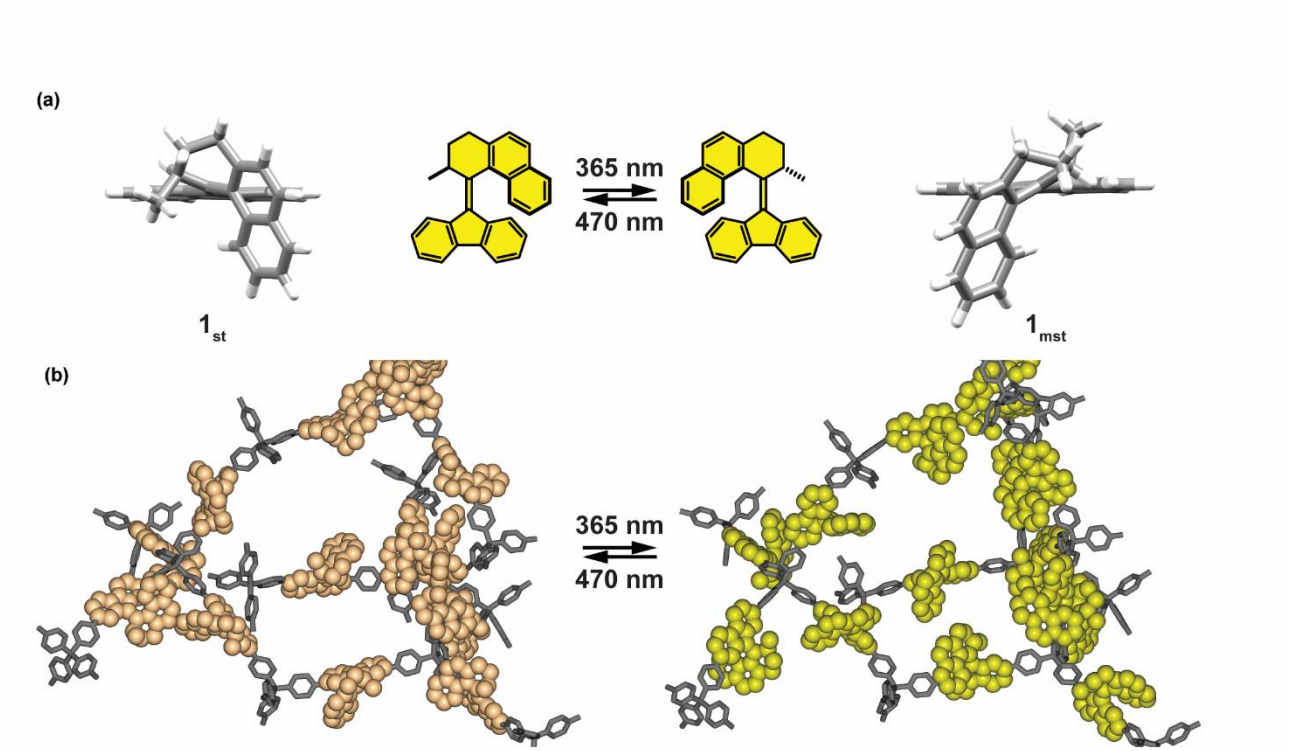

Figure 1. **Photoisomerization of overcrowded olefin-based bistable switch. a** Schematic representation of the structural changes upon photochemical E/Z isomerization of bistable overcrowded alkene **1** and top view of the DFT (B3LYP/631-G(d,p)) optimized structures of stable (**1st**, left) and metastable (**1mst**, right) isomers. **b** Schematic representation of photoswitching of overcrowded alkene **1** in pores of the PSF framework.

Synthesis of Porous Switchable Frameworks. The fabrication of robust porous materials with overcrowded alkene-based chiroptical switch **1st** directly inserted into the framework through covalent bonds was realized by a Yamamoto cross-coupling reaction. The reaction between a network-forming tri-dimensional monomer, tetra-*p*-bromo-phenylmethane (**TPM-Br4**), and an overcrowded alkene-based chiroptical switch **1st-Br2** bearing two bromide substituents afforded the desired frameworks (Figure 2a). The choice of the tetraphenyl methane (**TPM**) building block was motivated by the very high pore capacity and BET surface area up to ~5000 m^2/g of the **TPM**-based framework[24], which we envisaged to be suitable to provide a sufficient free volume for the isomerization of overcrowded alkene **1** embedded in the solid material. Two porous switchable frameworks (**PSFs)** were synthesized by varying the molar fraction of building blocks (**TPM** and **1**) used during the synthesis of the materials denoted as **PSF-1** and **PSF-2** (10:1 and 4:1 of **TPM-Br4** to **1st-Br2** for **PSF-1** and **PSF-2,** respectively, for synthetic details and characterization, see method section and supplementary information). The resulting PSFs were stable up to 450 °C, as determined by thermogravimetric analysis. The Langmuir and BET surface areas were 4545 and 3948 m^2/g for

PSF-1 and 1841 and 1616 m^2/g for **PSF-2** with pore capacity of 2.39 and 0.66 cm^3/g, respectively, while the pore size distribution was centred at about 1.4 nm for **PSF-1** and 1.2 nm for **PSF-2**, as calculated by non-Local Density Functional theory (Figure S11, Table S1). The homogeneity of the samples and the molecular composition of the frameworks were established by quantitative ^{13}C MAS NMR and the results correspond to the fractions of the building blocks used in the synthesis of the frameworks (Figure 2b, Figure S13).Thus, the fraction of the switch unit in the PSFs can be modulated at will, and **PSF-1** and **PSF-2** were used for further experiments.

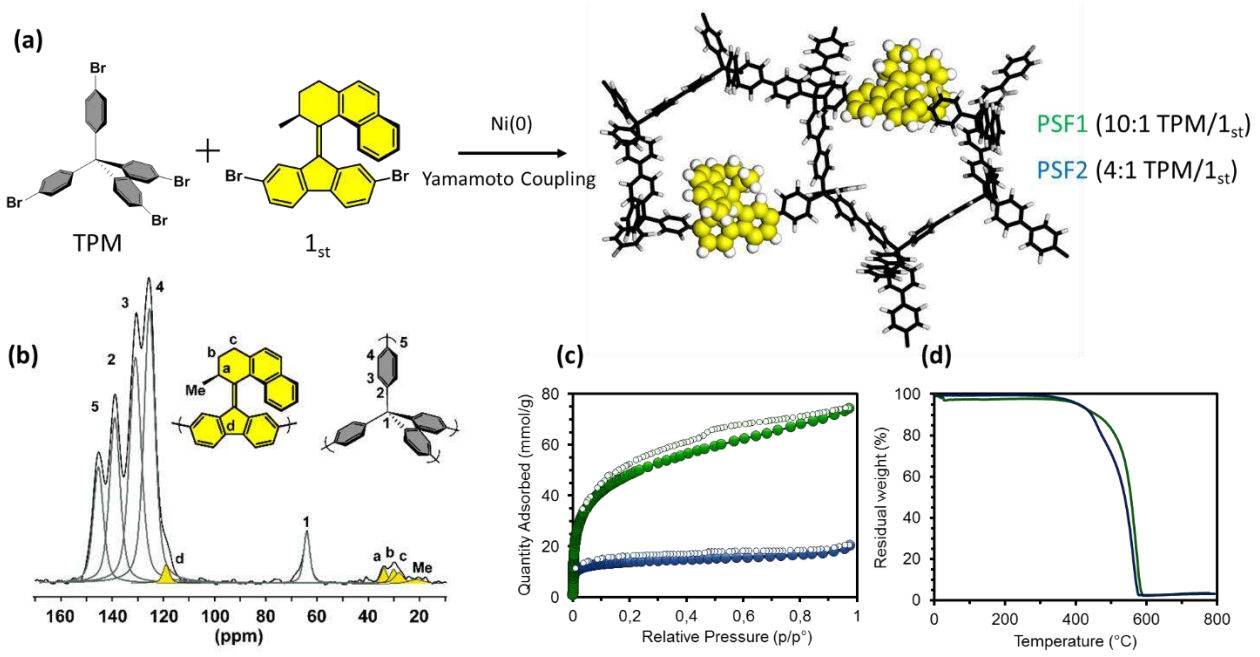

Figure 2. Synthesis of PSF materials. a Schematic representation of synthesis of the **PSF-1** and **PSF-2** materials from tetra-*p*-bromo-phenyl methane (**TPM-Br4**) and photoswitch **1st-Br2** via Yamamoto coupling. **b** Solid state ^{13}C MAS NMR (75.04 MHz, 12.5 kHz, recycle delay=100 s) spectrum of **PSF-2** material. **c** N_2 gas adsorption isotherms (77 K) of activated **PSF-1** (green trace) and **PSF-2** (blue isotherm). Filled and empty symbols denote adsorption and desorption, respectively. **d** TGA profiles of **PSF-1** (green line) and **PSF-2** (blue line).

Photochemical and thermal isomerization in solution The photochemical isomerization behaviour of **1st-Br2** in solution was studied with ^1H and ^{13}C NMR, UV/Vis absorption and Raman spectroscopies. In the ^1H NMR spectrum, irradiation of **1st-Br2** at 365 nm in CD_2Cl_2 solution resulted in appearance of a new set of ^1H downfield shifted resonances, indicating the formation of the metastable isomer (**1mst-Br2**) with almost quantitative yield (PSS_{365} 94:6 of **1mst-Br2**:**1st-Br2**) (Figure 3a, see Methods Section for details). Likewise, in the ^{13}C NMR spectrum, a new set of upfield shifted resonances for carbons C_a (35.6 → 34.6 ppm), and C_c (30.0 → 28.5 ppm) was observed, in line with the formation of **1mst-Br2** (Figure 3b). In the UV/Vis absorption spectrum, irradiation at 365 nm led to a gradual bathochromic shift of the absorption band centred at 366 nm. This shift of absorption is

consistent with the formation of the metastable twisted isomer of the overcrowded alkene-based photoswitch. During the photo-isomerization, an isosbestic point was maintained at 385 nm, indicating a unimolecular process (Figure 3c). In the Raman spectrum of **1st-Br2**, a band centred at 1582 cm^{-1} is present, characteristic of the stretching of the olefinic bond of the photoswitch **1st-Br2**. Upon irradiation of the sample at 365 nm, this band disappeared, while a new broad band centred at 1542 cm^{-1}, characteristic of the stretching of the olefinic bond of the metastable overcrowded alkene - **1mst-Br2** appeared. The reverse **1mst-Br2** → **1st-Br2** isomerization in solution could be achieved by irradiation of the **1mst** at 470 nm upon which the ^{1}H NMR resonances of **1st-Br2** reappeared (PSS_{470} 97:3 **1st-Br2** to **1mst-Br2**) (Figure S2,3) and the original UV/Vis absorption and Raman spectra were recovered (Figure 3c,d).

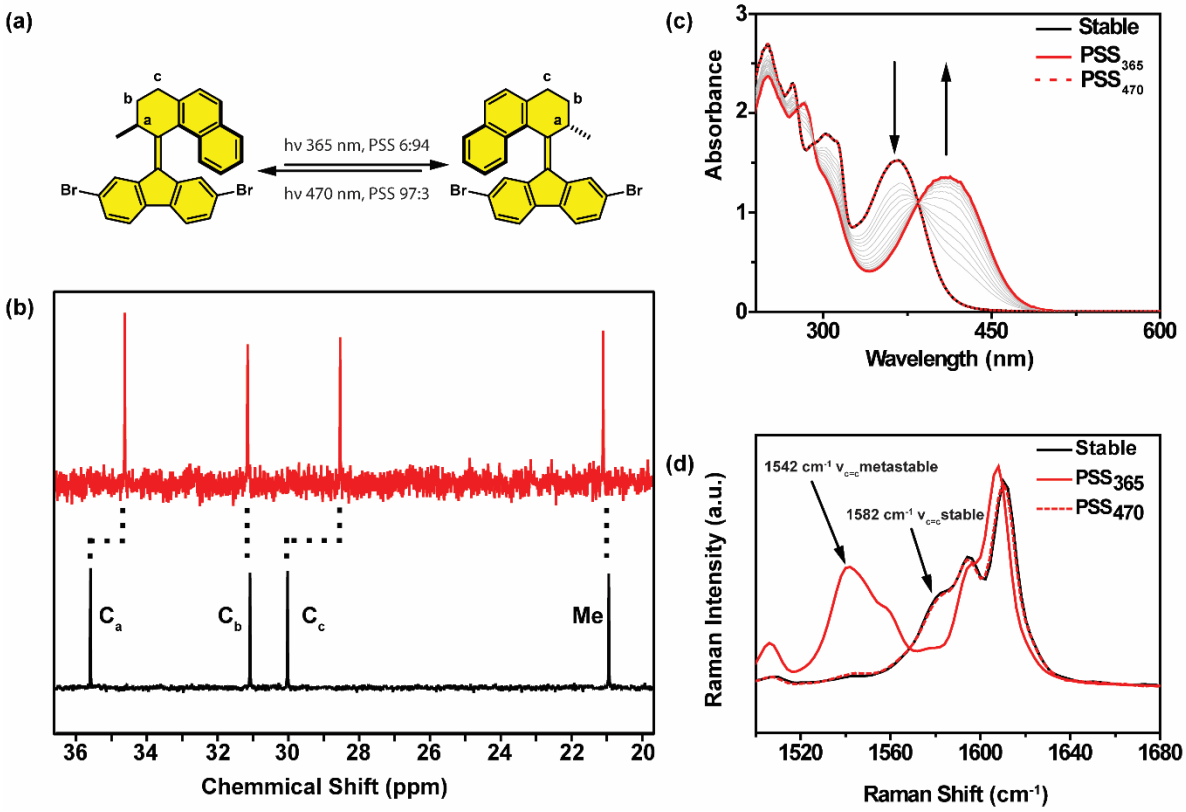

Figure 3. Photochemical isomerization of bistable switch 1 in solution. a Schematic representation of the structural change upon photochemical E/Z isomerization of overcrowded alkene based bistable switch **1**. **b** Comparison of aliphatic part of ^{13}C NMR (CD_2Cl_2, 400 MHZ, See Figure 3a for atom labelling) spectra of **1st** (black spectrum, bottom) and **1mst** (red spectrum, top). **c** Changes in UV/Vis spectra of **1st** (8 µM, DCM) upon irradiation at 365 nm and subsequent irradiation at 470 nm. **d** Comparison of Raman spectra (785 nm, 50 mW) of **1st** (black solid line), **1mst** as a photostationary state mixture obtained by irradiation of **1st** solution at 365 nm (red solid line, PSS_{365}) mixture, and PSS_{365} irradiated at 470 nm to recover **1st** (red dashed line, PSS_{470}) mixture drop-casted on quartz substrate.

Photochemical isomerization in the solid state. The photochemical isomerization behaviour (Figure 4a,b) of the switch **1** embedded in the solid **PSF-1** and **PSF-2** frameworks was studied with

Diffuse-Reflectance UV/Vis (DR UV/Vis) and Raman spectroscopies (Figure 4c-f). Upon exposure to light irradiation, spectral changes almost identical to those found in solution were detected for both porous materials (**PSF-1** and **PSF-2**) indicating facile photoisomerization of the overcrowded alkene embedded in the PSFs. In the DR UV/Vis spectra of **PSF-1** and **PSF-2,** bathochromic shifts were observed upon irradiation at 365 nm and hypsochromic shifts upon irradiation at 470 nm in line with the light reversible $\mathbf{1}_{mst} \leftrightarrow \mathbf{1}_{st}$ photoisomerization (Figure 4c and d, respectively). Additionally, the evident colour change from white to yellow of the material exposed to 365 nm light was readily visible, which is consistent with the bathochromic shift of the absorption spectra of the material (Figure 4b). For both materials, the alternating cycles of the UV and Visible light irradiations could be repeated for several cycles without any noticeable sign of fatigue indicating high stability of the material (Figure 4c and d insets for **PSF-1** and **PSF-2**, respectively). The Raman spectra of both solid **PSFs** were dominated by the intense broad band centred at 1610 cm^{-1} characteristic of the C=C stretching in the aromatic rings, associated with the relatively large fraction of **TPM** building blocks in both frameworks. Nevertheless, irradiation of the porous materials at 365 nm resulted in the expected decrease in Raman intensity at 1582 cm^{-1} and the appearance of a distinctive new band at 1542 cm^{-1}. Irradiation at 470 nm fully reverted these changes for the **PSF-1** framework as the band characteristic of the $\mathbf{1}_{mst}$ isomer could not be detected in the Raman spectrum, clearly demonstrating the reversible photoisomerization of **1** incorporated in the solid material (Figure 4e). Conversely, **1** incorporated in the **PSF-2** framework showed only a partial back-isomerization to $\mathbf{1}_{st}$ upon irradiation at 470 nm, as indicated by the incomplete disappearance of the band at 1542 cm^{-1}. Complete reversibility occurred by thermal treatment as shown below.

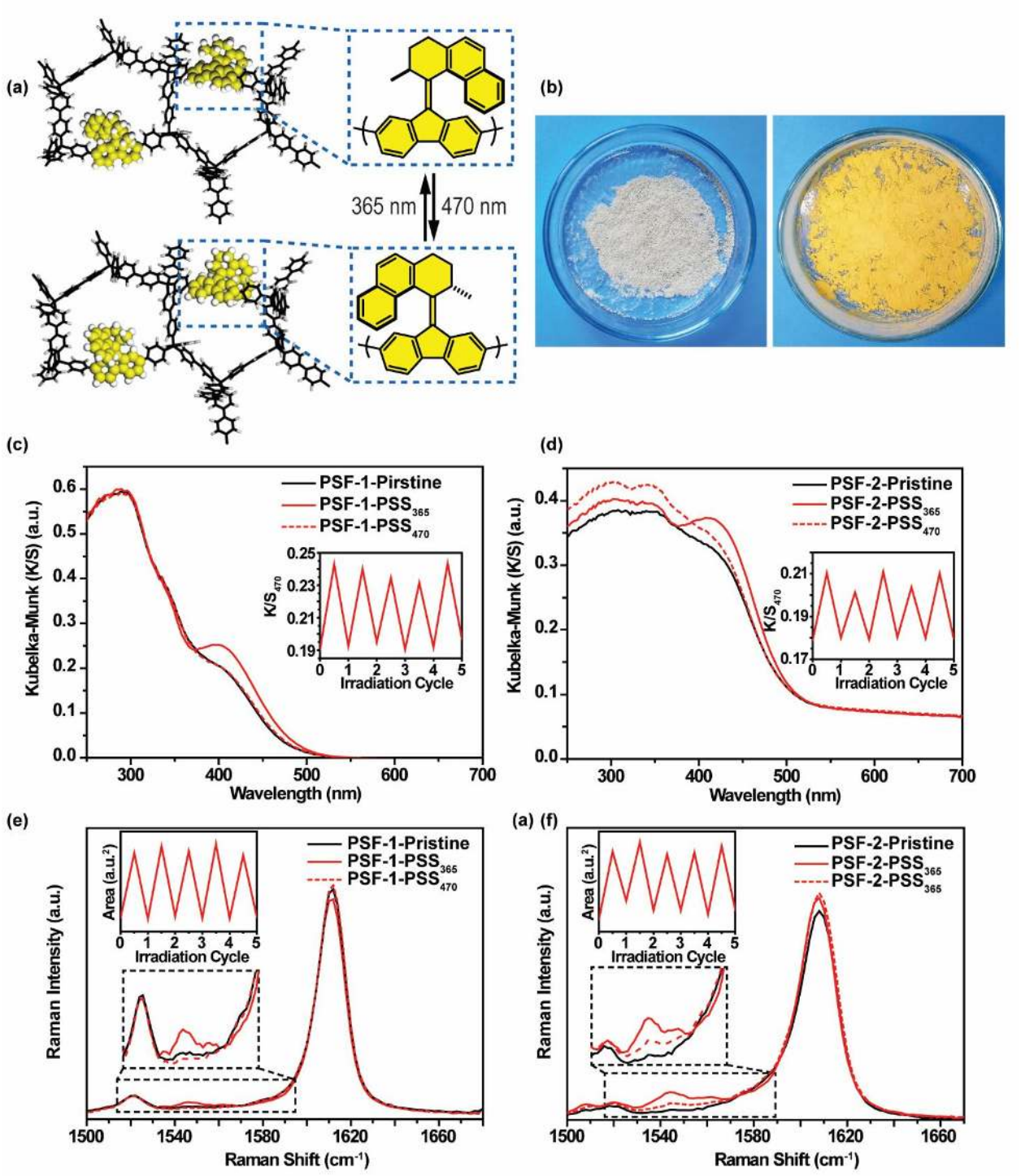

Figure 4. Photochemical isomerization studies in the solid state, a Schematic representation of light-induced structural changes in the PSFs upon isomerization of **1** from stable to metastable isomer, **b** Pictures of the **PSF-2** material before (left panel) and after (right panel) irradiation at 365 nm for 30 min (power density ~ 20 mW/cm^2). **c,d** Changes in the diffuse-reflectance UV/Vis spectra of the PSFs (**PSF-1** - panel **c**, **PSF-2** - panel **d**) materials upon consecutive irradiation at 365 nm followed by irradiation at 470 nm for 45 min (power density ~ 8 mW/cm^2). Pristine materials (black, solid lines, pristine), photostationary state reached upon irradiation at 365 nm (red, solid line, PSS_{365}), and photostationary state reached upon subsequent irradiation of the material at 470 nm (red, dashed lines, PSS_{470}). The insets show changes in the Kubelka-Munk function at 470 nm over alternative irradiation cycles. **e,f** Changes in the Raman spectra (785 nm, 50 mW) of PSFs (**PSF-1** - panel **e**, **PSF-2** - panel

f materials consecutive irradiation at 365 nm followed by irradiation at 470 nm. Pristine materials (black, solid lines, pristine), photostationary state reached upon irradiation at 365 nm (red, solid lines, PSS_{365}), and photostationary state reached upon subsequent irradiation of the material at 470 nm (red, dashed lines, PSS_{470}). The insets show changes in the area of the band centred at 1547 cm^{-1} over alternative irradiation cycles.

Solid state ^{13}C MAS NMR has proven to be a technique sensitive to the structural changes occurring to the individual components of the framework at a molecular level, thus providing a precise tool to quantify the extent of photoisomerization in the bulk of the material. For the solid state NMR studies the **PSF-2** framework was chosen owing to its higher content of the photoswitch **1**, which facilitated quantitative analysis of the spectra. To this end, the **PSF-2** material was irradiated at 365 nm with low power density (~3 mW/cm^2 for 54 h) and ^{13}C MAS NMR spectra were recorded. Upon irradiation of **PSF-2** at 365 nm similar changes to those observed in solution were recorded, that is, the upfield shift of the resonances of the carbons C_a (35.0 → 34.1 ppm), and C_c (29.2 → 28.0 ppm) (Figure 5b). This similarity to the solution studies allowed us to unequivocally ascribe these changes to photochemical formation of the metastable isomer ($\mathbf{1_{mst}}$) embedded in the framework, in agreement with DR UV/Vis and Raman spectral data (Figure 4). Deconvolution of the spectrum and integration of the resonances originating from the respective diastereoisomers (Figure 5b middle panel, Table S4) showed that the photostationary state achieved upon irradiation of the bulk material (93:7 of $\mathbf{1_{mst}}$:$\mathbf{1_{st}}$) is as high as that in solution (94:6 of $\mathbf{1_{mst}}$:$\mathbf{1_{st}}$). This observation is remarkable as bulk photoswitching of solid materials have been previously reported only for flexible MOFs containing dithienylethenes derived struts[42,45] and porous molecular crystals sustained by weak van der Waals interactions.[29] Upon irradiation at 470 nm, the metastable form reverted only partially to the stable form as determined by solid state NMR (Figure S15, Table S4) and in accordance with Raman spectroscopy results; however, upon thermal treatment, the metastable isomer could be quantitatively converted into the $\mathbf{1_{st}}$, as shown by the recovery of the original ^{13}C MAS NMR spectrum (Figure 5b right panel).

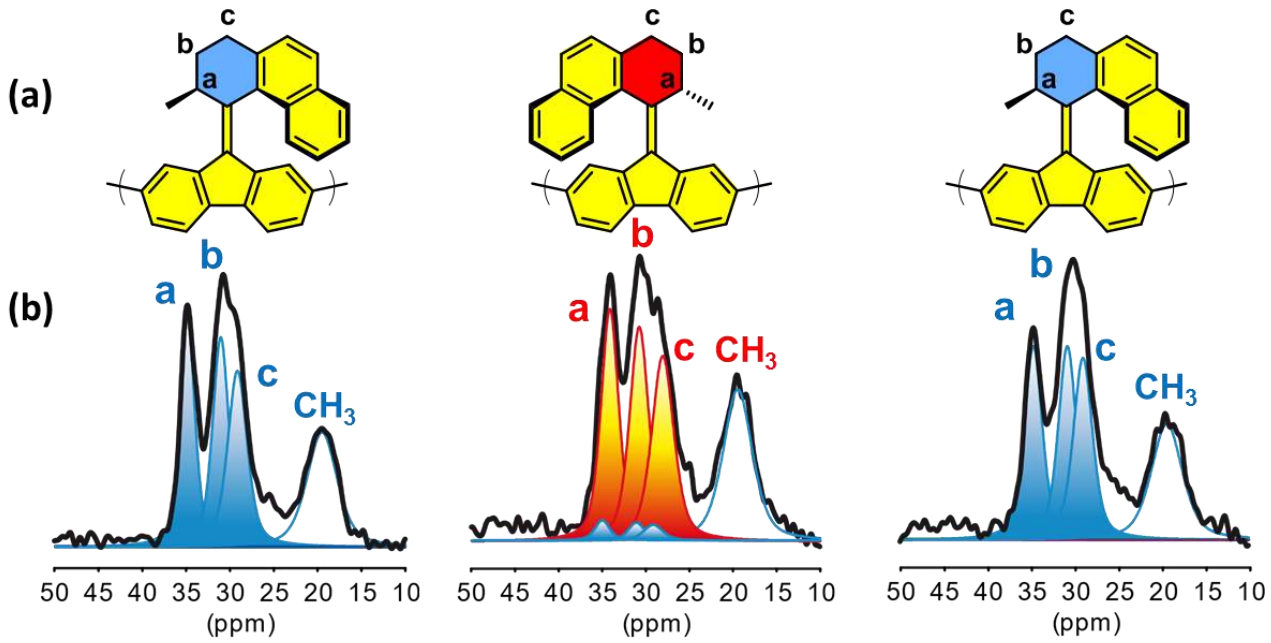

Figure 5. a Schematic representation of the structural changes of **1** (**1**$_{st}$) (left) incorporated in the **PSF-2** framework upon irradiation at 365 nm (**1**$_{mst}$) (middle) and subsequent heating (**1**$_{st}$) (right). **b** Changes in the $^{13}C\{^{1}H\}$ CP-MAS NMR spectra of the **PSF-2** framework at each stage of the structural transformations, pristine (left), after photoisomerization (middle) and thermal annealing (right).

Gas adsorption experiments. We anticipated that the accessible volume of the framework would be reversibly changed during the overall stable-metastable-stable isomerization sequence and therefore, gas adsorption experiments were performed. Indeed, N_2 adsorption isotherms at 77 K revealed a striking reduction of the pore volume between pristine and irradiated **PSF-2** material, which accounts for 20% at $p/p°$=0.6 (Figure 6). This value was confirmed by CO_2 adsorption isotherms at 195 K (from 500.2 to 402 cm^3/g STP, Figure S12). Furthermore, this phenomenon was reversible after heating of the irradiated material, as demonstrated by N_2 adsorption isotherm (Figure 6c). The differences in the observed porosity of the material upon isomerization of **1** can be rationalized by the volume change that the switch occupies in the framework upon photoisomerization. The structures and geometries of both stable and metastable isomers were optimized by DFT on the B3LYP 6-31G(d,p) level of theory. While the stable isomer adopts a folded conformation in which both methyl and naphthyl substituents are located on the same side of the central olefinic bond, the steric congestion in the metastable isomer forces the molecule to adopt a twisted conformation. As a result the dihedral angles between substituents of the central double bond increase from 13.4° and 14.4° in **1**$_{st}$ to 25.2° and 27.3° for **1**$_{mst}$. Based on these results, we hypothesized that the photogenerated **1**$_{mst}$ occupies larger volume in comparison to **1**$_{st}$ due to the mismatch of the twisted conformation with the surrounding framework, thus partially reducing the accessible volume of the pores and the gas uptake.

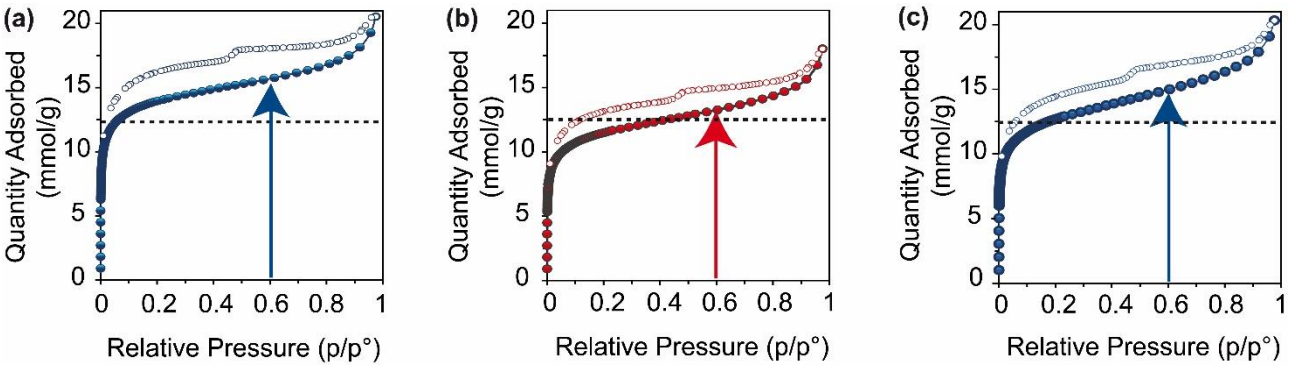

Figure 6. Switching of the gas adsorption properties. N_2 adsorption isotherms of the **PSF-2** framework at 77 K of the pristine material (a, blue isotherm), after irradiation at 365 nm for 54 h (b, red isotherm) and heating (c, blue isotherm). The filled and open circles denote adsorption and desorption isotherms, respectively.

Conclusions In conclusion, we have developed a convenient strategy in which overcrowded alkene based photoswitches are covalently incorporated in solid and robust porous materials. Two porous switchable frameworks consisting of a tetraphenylmethane moiety (**TPM**) and various amounts of photoswitch were obtained by the formation of carbon-carbon bonds, such that the switch is an intrinsic part of the framework itself, without reducing its interconversion efficiency. The great stability of the solid state framework, combined with the dynamics of light-responsive switches were proven to modulate gas sorption, yet retaining high porosity in each respective geometry. Such unique prerogative of high porosity for both states of the bi-stable switch, provided by our strategy of using highly porogenic tetraphenylmethane building blocks, was crucial for unhindered reversible photoisomerization in the solid state. Combining Diffuse-Reflectance UV/Vis and Raman spectroscopies, it was demonstrated that the chiroptical switch embedded in the porous framework maintains its function and can undergo frequency-dependent isomerization upon exposure to light. Furthermore, solid-state NMR studies performed on the framework with higher photoswitch content showed that the photostationary state ratio of the chiroptical switch **1** inserted in the framework, as established in the solid sample upon exposure to UV irradiation, is essentially the same as the one reached in solution. These findings are highly remarkable since the values of the photostationary state previously reported for bulk solid materials had never been as high as in solution. Furthermore, the porosity and gas uptake of the **PSF-2** material can be reversibly modulated with light and heat. The novel prototypical material allow us to envision the generation of responsive properties of practical utility, such as the regulation of adsorption on command. Indeed, our findings open up opportunities

to apply these novel materials, among others, in controlled gas uptake and release, as well as switchable size-based or enantiomer-based[62] separations technologies.

1. Dietrich-Buchecker, C., Jimenez-Molero, M. C., Sartor, V. & Sauvage, J.-P. Rotaxanes and catenanes as prototypes of molecular machines and motors. *Pure Appl. Chem.* **75,** 1383–1393 (2003).
2. Balzani, V., Venturi, M. & Credi, A. *Molecular devices and machines : a journey into the nano world*. (Wiley-VCH, 2003).
3. Kay, E. R., Leigh, D. A. & Zerbetto, F. Synthetic molecular motors and mechanical machines. *Angew. Chem. Int. Ed.* **46,** 72–191 (2007).
4. Erbas-Cakmak, S., Leigh, D. A., McTernan, C. T. & Nussbaumer, A. L. Artificial Molecular Machines. *Chem. Rev.* **115,** 10081–10206 (2015).
5. Browne, W. R. & Feringa, B. L. Making molecular machines work. *Nat. Nanotechnol.* **1,** 25–35 (2006).
6. Kinbara, K. & Aida, T. Toward Intelligent Molecular Machines: Directed Motions of Biological and Artificial Molecules and Assemblies. *Chem. Rev.* **105,** 1377–1400 (2005).
7. Astumian, R. D., R., Kay, E. R., Leigh, D. A. & Zerbetto, F. Design principles for Brownian molecular machines: how to swim in molasses and walk in a hurricane. *Proc. Natl. Acad. Sci., U. S. A* **46,** 10771–10776 (2006).
8. Coskun, A., Banaszak, M., Astumian, R. D., Stoddart, J. F. & Grzybowski, B. A. Great expectations: can artificial molecular machines deliver on their promise? *Chem. Soc. Rev.* **41,** 19–30 (2012).
9. Astumian, R. D. How molecular motors work – insights from the molecular machinist's toolbox: the Nobel prize in Chemistry 2016. *Chem. Sci.* **8,** 840–845 (2017).
10. van Leeuwen, T., Lubbe, A. S., Štacko, P., Wezenberg, S. J. & Feringa, B. L. Dynamic control of function by light-driven molecular motors. *Nat. Rev. Chem.* **1,** 0096 (2017).
11. Furukawa, H., Cordova, K. E., O'Keeffe, M. & Yaghi, O. M. The chemistry and applications of metal-organic frameworks. *Science* **341,** 1230444 (2013).
12. Howarth, A. J. *et al.* Chemical, thermal and mechanical stabilities of metal-organic frameworks. *Nat. Rev. Mater.* **1,** 1–15 (2016).
13. Kitagawa, S., Kitaura, R. & Noro, S. Functional porous coordination polymers. *Angew. Chem. Int. Ed.* **43**, 2334-2375 (2004).
14. Diercks, C. S. & Yaghi, O. M. The atom, the molecule, and the covalent organic framework. *Science* **355,** eaal1585 (2017).
15. Das, S., Heasman, P., Ben, T. & Qiu, S. Porous organic materials: strategic design and structure-function correlation. *Chem. Rev.* **117**, 1515-1563 (2017).
16. Gould, S. L., Tranchemontagne, D., Yaghi, O. M. & Garcia-Garibay, M. A. The Amphidynamic Character of Crystalline MOF-5 : Rotational Dynamics in a Free-Volume Environment. *J. Am. Chem. Soc.* **130,** 3246–3247 (2008).

17. Vogelsberg, C. S. *et al.* Ultrafast rotation in an amphidynamic crystalline metal organic framework. *Proc. Natl. Acad. Sci.* **114,** 13613–13618 (2017).

18. Comotti, A., Bracco, S. & Sozzani, P. Molecular rotors built in porous materials. *Acc. Chem. Res.* **49**, 1701-1710 (2016).

19. Bracco, S. *et al.* CO_2 regulates molecular rotor dynamics in porous materials. *Chem. Commun.* **53,** 7776–7779 (2017).

20. Bracco, S. *et al.* Ultrafast Molecular Rotors and Their CO_2 Tuning in MOFs with Rod-Like Ligands. *Chem. Eur. J.* **23,** 11210–11215 (2017).

21. Vukotic, V. N., Harris, K. J., Zhu, K., Schurko, R. W. & Loeb, S. J. Metal-organic frameworks with dynamic interlocked components. *Nat. Chem.* **4,** 456–460 (2012).

22. Vukotic, V. N. *et al.* Mechanically Interlocked Linkers inside Metal − Organic Frameworks : Effect of Ring Size on Rotational Dynamics. *J. Am. Chem. Soc.* **137,** 9643–9651 (2015).

23. Comotti, A., Bracco, S., Ben, T., Qiu, S. & Sozzani, P. Molecular Rotors in Porous Organic Frameworks. *Angew. Chem. Int. Ed.* **53,** 1043–1047 (2014).

24. Zhu, K., O'Keefe, C. A., Vukotic, V. N., Schurko, R. W. & Loeb, S. J. A molecular shuttle that operates inside a metal-organic framework. *Nat. Chem.* **7,** 514–519 (2015).

25. Chen, Q. *et al.* A Redox-Active Bistable Molecular Switch Mounted inside a Metal-Organic Framework. *J. Am. Chem. Soc.* **138,** 14242–14245 (2016).

26. Danowski, W. *et al.* Unidirectional rotary motion in a metal–organic framework. *Nat. Nanotechnol.* **14,** 488–494 (2019).

27. Coudert, F. X. Responsive metal-organic frameworks and framework materials: Under pressure, taking the heat, in the spotlight, with friends. *Chem. Mater.* **27,** 1905–1916 (2015).

28. Castellanos, S., Kapteijn, F. & Gascon, J. Photoswitchable metal organic frameworks: Turn on the lights and close the windows. *CrystEngComm* **18,** 4006–4012 (2016).

29. Baroncini, M. *et al*. Photoinduced reversible switching of porosity in molecular crystals based on star-shaped azobenzene tetramers. *Nature Chem.* **7**, 634-640.

30. Wang, Z. *et al.* Series of Photoswitchable Azobenzene-Containing Metal-Organic Frameworks with Variable Adsorption Switching Effect. *J. Phys. Chem. C* **122,** 19044–19050 (2018).

31. Prasetya, N., Donose, B. C. & Ladewig, B. P. A new and highly robust light-responsive Azo-UiO-66 for highly selective and low energy post-combustion CO_2 capture and its application in a mixed matrix membrane for CO_2/N_2 separation. *J. Mater. Chem. A* **6,** 16390–16402 (2018).

32. Castellanos, S. *et al.* Structural Effects in Visible-Light-Responsive Metal-Organic Frameworks Incorporating ortho-Fluoroazobenzenes. *Chem. Eur. J.* **22,** 746–752 (2016).

33. Brown, J. W. *et al.* Photophysical pore control in an azobenzene-containing metal–organic framework. *Chem. Sci.* **4,** 2858 (2013).

34. Gong, L. Le, Feng, X. F. & Luo, F. Novel azo-Metal-Organic Framework Showing a 10-Connected bct Net, Breathing Behavior, and Unique Photoswitching Behavior toward CO2. *Inorg. Chem.* **54,** 11587–11589 (2015).

35. Heinke, L. *et al.* Photoswitching in two-component surface-mounted metal-organic

frameworks: Optically triggered release from a molecular container. *ACS Nano* **8,** 1463–1467 (2014).

36. Lyndon, R. *et al.* Dynamic photo-switching in metal-organic frameworks as a route to low-energy carbon dioxide capture and release. *Angew. Chem. Int. Ed.* **52,** 3695–3698 (2013).

37. Wang, Z. *et al.* Tunable molecular separation by nanoporous membranes. *Nat. Commun.* **7,** 1–7 (2016).

38. Yu, X. *et al.* Cis-to-trans isomerization of azobenzene investigated by using thin films of metal-organic frameworks. *Phys. Chem. Chem. Phys.* **17,** 22721–22725 (2015).

39. Park, J. *et al.* Reversible alteration of CO_2 adsorption upon photochemical or thermal treatment in a metal-organic framework. *J. Am. Chem. Soc.* **134,** 99–102 (2012).

40. Walton, I. M. *et al.* Photo-responsive MOFs: Light-induced switching of porous single crystals containing a photochromic diarylethene. *Chem. Commun.* **49,** 8012–8014 (2013).

41. Patel, D. G. *et al.* Photoresponsive porous materials: The design and synthesis of photochromic diarylethene-based linkers and a metal-organic framework. *Chem. Commun.* **50,** 2653–2656 (2014).

42. Nikolayenko, V. I., Herbert, S. A. & Barbour, L. J. Reversible structural switching of a metal-organic framework by photoirradiation. *Chem. Commun.* **53,** 11142–11145 (2017).

43. Fan, C. Bin *et al.* Significant Enhancement of C_2H_2/C_2H_4 Separation by a Photochromic Diarylethene Unit: A Temperature- and Light-Responsive Separation Switch. *Angew. Chem. Int. Ed.* **56,** 7900–7906 (2017).

44. Luo, F. *et al.* Photoswitching CO_2 capture and release in a photochromic diarylethene metal-organic framework. *Angew. Chem. Int. Ed.* **53,** 9298–9301 (2014).

45. Zheng, Y. *et al.* Flexible interlocked porous frameworks allow quantitative photoisomerization in a crystalline solid. *Nat. Commun.* **8,** 1–6 (2017).

46. Williams, D. E. *et al.* Energy Transfer on Demand: Photoswitch-Directed Behavior of Metal–Porphyrin Frameworks. *J. Am. Chem. Soc.* **136,** 11886–11889 (2014).

47. Furlong, B. J. & Katz, M. J. Bistable Dithienylethene-Based Metal-Organic Framework Illustrating Optically Induced Changes in Chemical Separations. *J. Am. Chem. Soc.* **139,** 13280–13283 (2017).

48. Irie, M., Fukaminato, T., Matsuda, K. & Kobatake, S. Photochromism of diarylethene molecules and crystals: Memories, switches, and actuators. *Chem. Rev.* **114,** 12174–12277 (2014).

49. Kolokolov, D. I. *et al.* Flipping the Switch: Fast Photoisomerization in a Confined Environment. *J. Am. Chem. Soc.* **140,** 7611–7622 (2018).

50. Dolgopolova, E. A. *et al.* Connecting Wires: Photoinduced Electronic Structure Modulation in Metal-Organic Frameworks. *J. Am. Chem. Soc.* **141,** 5350–5358 (2019).

51. Kundu, P. K., Olsen, G. L., Kiss, V. & Klajn, R. Nanoporous frameworks exhibiting multiple stimuli responsiveness. *Nat. Commun.* **5,** 1–9 (2014).

52. Koumura, N., Zijistra, R. W. J., van Delden, R. A., Harada, N. & Feringa, B. L. Light-driven monodirectional molecular rotor. *Nature* **401,** 152–155 (1999).

53. Koumura, N., Geertsema, E. M., Meetsma, A. & Feringa, B. L. Light-driven molecular rotor: Unidirectional rotation controlled by a single stereogenic center. *J. Am. Chem. Soc.* **122,** 12005–12006 (2000).

54. Kistemaker, J. C. M., Pizzolato, S. F., van Leeuwen, T., Pijper, T. C. & Feringa, B. L. Spectroscopic and Theoretical Identification of Two Thermal Isomerization Pathways for Bistable Chiral Overcrowded Alkenes. *Chem. Eur. J.* **22,** 13478–13487 (2016).

55. Iamsaard, S. *et al.* Conversion of light into macroscopic helical motion. *Nat. Chem.* **6,** 229–235 (2014).

56. Orlova, T. *et al.* Revolving supramolecular chiral structures powered by light in nanomotor-doped liquid crystals. *Nat. Nanotechnol.* **13,** 304–308 (2018).

57. Eelkema, R. *et al.* Nanomotor rotates microscale objects. *Nature* **440,** 163 (2006).

58. Chen, J. *et al.* Artificial muscle-like function from hierarchical supramolecular assembly of photoresponsive molecular motors. *Nat. Chem.* **10,** 132–138 (2018).

59. Li, Q. *et al.* Macroscopic contraction of a gel induced by the integrated motion of light-driven molecular motors. *Nat. Nanotechnol.* **10,** 161–165 (2015).

60. Foy, J. T. *et al.* Dual-light control of nanomachines that integrate motor and modulator subunits. *Nat. Nanotechnol.* **12,** 540–545 (2017).

61. Chen, K. Y. *et al.* Control of surface wettability using tripodal light-activated molecular motors. *J. Am. Chem. Soc.* **136,** 3219–3224 (2014).

62. Shimomura, K., Ikai, T., Kanoh, S., Yashima, E. & Maeda, K. Switchable enantioseparation based on macromolecular memory of a helical polyacetylene in the solid state. *Nat. Chem.* **6,** 429–434 (2014).

Data availability. The data associated with the reported findings are available in the manuscript or the Supplementary Information. Other related data are available from the corresponding author upon request.

Acknowledgements

This work was supported financially by the Netherlands Organization for Scientific Research (NWO-CW), the European Research Council (ERC, advanced grant no. 694345 to B.L.F.), the Ministry of Education, Culture and Science (Gravitation Program no. 024.001.035), We thank the University of Groningen for access to the Peregrine Computing Cluster. A.C. and P.S. acknowledges Ministero dell'Istruzione, dell'Università e della Ricerca (MIUR - Progetto Dipartimento di Eccellenza 2018-2022), PRIN 2016-NAZ-0104 and PRIN 2018 (NEMO) for financial support.

Author contributions

W.D., F.C., S.J.W., P.S. and B.L.F. conceived the project. W.D. synthesized bistable switch **1-Br$_2$,** F.C. synthesized **PSF** materials. W.D. performed photoisomerization studies in solution, Raman and DR UV/Vis studies on PSFs. S.B. and A.C. performed SS NMR studies on synthesized materials. F.C. performed DSC, TGA and gas uptake experiments. W.D. performed DFT studies. S.J.W., A.C. and B.L.F. guided the project. W.D., A.C., S.J.W., P.S., B.L.F. wrote the manuscript. All authors discussed the results and commented on the manuscript.

Additional information

Supplementary information and chemical compound information are available in the online version of the paper. Reprints and permissions information is available online at www.nature.com/reprints. Correspondence and requests for materials should be addressed to S.J.W., A.C., or B.L.F.

Competing financial interests

The authors declare no competing financial interests.